ANALYSIS AND SIMULATION OF FAR-FIELD SEISMIC DATA FROM THE SOURCE PHYSICS EXPERIMENT

Arben Pitarka, Robert J. Mellors, Arthur J. Rodgers, Sean R. Ford, Phillip E. Harben, Jeffery L. Wagoner, William R. Walter, Michael E. Pasyanos, Anders Petersson, Oleg Y. Vorobiev, Heming Xu, Stan D. Ruppert, Stephen C. Myers, Eric M. Matzel, and Douglas A. Dodge

Lawrence Livermore National Laboratory

Sponsored by the National Nuclear Security Administration

Award No. DE-AC52-06NA25946/NST11-NCNS-TM-EXP-PD15

ABSTRACT

The Source Physics Experiment (SPE-N) at the Nevada National Security Site (NNSS) provides new data for investigating the excitation and propagation of seismic waves generated by buried explosions. A particular target is the generation of S waves. The far-field ground motions during the first two SPE explosions reveal complex features, such as pronounced azimuthal variations in P- and S-wave arrival times, amplitudes and scattered energy. Substantial energy is observed on the tangential component. We pursue multiple approaches for analyzing the effects of three-dimensional (3D) structure and scattering on wave propagation. These include determinations of the source characteristics, comparisons of waveforms from local earthquakes with the SPE waveforms, refinements of the 3D velocity model, and numerical simulations of the source using both standard moment tensor representations and coupled hydrodynamic codes. A comparison of the SPE waveforms with nearby earthquakes shows clear differences in phase amplitude ratios between the shots and the earthquakes. A full waveform moment tensor inversion using a 1D velocity model and seismograms recorded at a distance of approximately 2 km yielded a poor fit to the tangential components suggesting significant 3D velocity variations. Anelastic finite-difference synthetic seismograms were calculated using the WPP computer program and a 3D seismic model. The 3D seismic model includes surface topography. It is based on regional geological data, with material properties constrained by shallow borehole data. The model was progressively increased in complexity by adding random heterogeneities to evaluate the effect of wave scattering on waveform complexity. Two types of sources were tested: a moment tensor representation and an extended source generated by GEODYN, which is a 3D hydro-dynamic code. Finally we use simulations of the SPE explosions and local earthquakes to examine the frequency behavior of P/S ratios as function of source size and geology.

Report Documentation Page

Form Approved
OMB No. 0704-0188

1. REPORT DATE	2. REPORT TYPE	3. DATES COVERED
SEP 2012		**00-00-2012 to 00-00-2012**

4. TITLE AND SUBTITLE	5a. CONTRACT NUMBER
Analysis and Simulation of Far-Field Seismic Data from the Source Physics Experiment	5b. GRANT NUMBER
	5c. PROGRAM ELEMENT NUMBER
6. AUTHOR(S)	5d. PROJECT NUMBER
	5e. TASK NUMBER
	5f. WORK UNIT NUMBER
7. PERFORMING ORGANIZATION NAME(S) AND ADDRESS(ES) **Lawrence Livermore National Laboratory,7000 East Ave,Livermore,CA,94550-9234**	8. PERFORMING ORGANIZATION REPORT NUMBER
9. SPONSORING/MONITORING AGENCY NAME(S) AND ADDRESS(ES)	10. SPONSOR/MONITOR'S ACRONYM(S)
	11. SPONSOR/MONITOR'S REPORT NUMBER(S)

12. DISTRIBUTION/AVAILABILITY STATEMENT

Approved for public release; distribution unlimited

13. SUPPLEMENTARY NOTES

Published in the Proceedings of the 2012 Monitoring Research Review - Ground-Based Nuclear Explosion Monitoring Technologies, 18-20 September 2012, Albuquerque, NM. Volume II. Sponsored by the Air Force Research Laboratory (AFRL) and the National Nuclear Security Administration (NNSA). U.S. Government or Federal Rights License

14. ABSTRACT

The Source Physics Experiment (SPE-N) at the Nevada National Security Site (NNSS) provides new data for investigating the excitation and propagation of seismic waves generated by buried explosions. A particular target is the generation of S waves. The far-field ground motions during the first two SPE explosions reveal complex features, such as pronounced azimuthal variations in P- and S-wave arrival times, amplitudes and scattered energy. Substantial energy is observed on the tangential component. We pursue multiple approaches for analyzing the effects of three-dimensional (3D) structure and scattering on wave propagation. These include determinations of the source characteristics, comparisons of waveforms from local earthquakes with the SPE waveforms, refinements of the 3D velocity model, and numerical simulations of the source using both standard moment tensor representations and coupled hydrodynamic codes. A comparison of the SPE waveforms with nearby earthquakes shows clear differences in phase amplitude ratios between the shots and the earthquakes. A full waveform moment tensor inversion using a 1D velocity model and seismograms recorded at a distance of approximately 2 km yielded a poor fit to the tangential components suggesting significant 3D velocity variations. Anelastic finite-difference synthetic seismograms were calculated using the WPP computer program and a 3D seismic model. The 3D seismic model includes surface topography. It is based on regional geological data, with material properties constrained by shallow borehole data. The model was progressively increased in complexity by adding random heterogeneities to evaluate the effect of wave scattering on waveform complexity. Two types of sources were tested: a moment tensor representation and an extended source generated by GEODYN which is a 3D hydro-dynamic code. Finally we use simulations of the SPE explosions and local earthquakes to examine the frequency behavior of P/S ratios as function of source size and geology.

15. SUBJECT TERMS

16. SECURITY CLASSIFICATION OF:			17. LIMITATION OF ABSTRACT	18. NUMBER OF PAGES	19a. NAME OF RESPONSIBLE PERSON
a. REPORT	b. ABSTRACT	c. THIS PAGE			
unclassified	**unclassified**	**unclassified**	**Same as Report (SAR)**	**10**	

OBJECTIVES

The SPE-N is a series of chemical explosions intended to enhance our physical understanding and ability to quantitatively model seismic signals from explosions at the NNSS with the goal of improving our nuclear test monitoring capabilities (Brunish et al., 2010). The main objective is to develop comprehensive three-dimensional high fidelity modeling capabilities to enable a transition from the current empirically-based explosion monitoring approach, where accuracy hinges on the availability of calibration data, to a physics-based predictive approach, where seismic observables are correlated to both non-linear physical processes in the near source region, and wave propagation scattering away from the source. To address these issues, we are developing an end-to-end three-dimensional (3D) simulation methodology to model the data collected, including non-linear (shock) motions and linear anelastic motions in the solid earth. We seek to understand the partitioning of energy excited by underground explosions and its propagation in complex 3D geological structure to far-field seismic monitoring stations. The data obtained during the SPE series will be used to validate and calibrate these numerical modeling techniques. Although the entire wavefield will be modeled, particular focus is on the generation of shear waves.

In parallel with the numerical modeling, a comprehensive set of empirical and semi-empirical analysis and discrimination techniques are being applied and will be contrasted with the numerical results. Here we present an overview of the research performed, which included signal analysis of ground motion data recorded at source distances shorter than 1 km, effects of underground structure on ground motion, full waveform moment tensor inversion of far-field motion for the SPE-2 explosion, analysis of P/S ratio as a function of source size using waveforms from SPE and local earthquakes. Finally we present preliminary results of our work on coupling three-dimensional near-field with far-field motion simulated with GEODYN and WPP computer programs developed at Lawrence Livermore National Laboratory.

RESEARCH ACCOMPLISHED

Analysis of Recorded Waveforms

A variety of instruments were deployed in five lines extending radially away from the shot point (Figure 1). Short-period (4.5 Hz) geophones, broad-band sensors, accelerometers and rotational sensors were deployed at selected locations. These instruments were installed on concrete pads set at a shallow depth into the surface.

Figure 2 shows recorded vertical component seismo-grams for two lines, Line 1 (L1) and Line 3 (L3), which show significant differences in amplitude and frequency. L1 is entirely situated on the weathered granite of the Climax Stock, while L3 starts on the granite but is mostly situated on the Quaternary sediments in the northern Yucca Flat basin. Seismograms on L1 show relatively constant moveout and clear Rg waves with a low phase velocity (about 600 m/s). The ground motion recorded along L3 is more complex and likely due to the transition from the granite

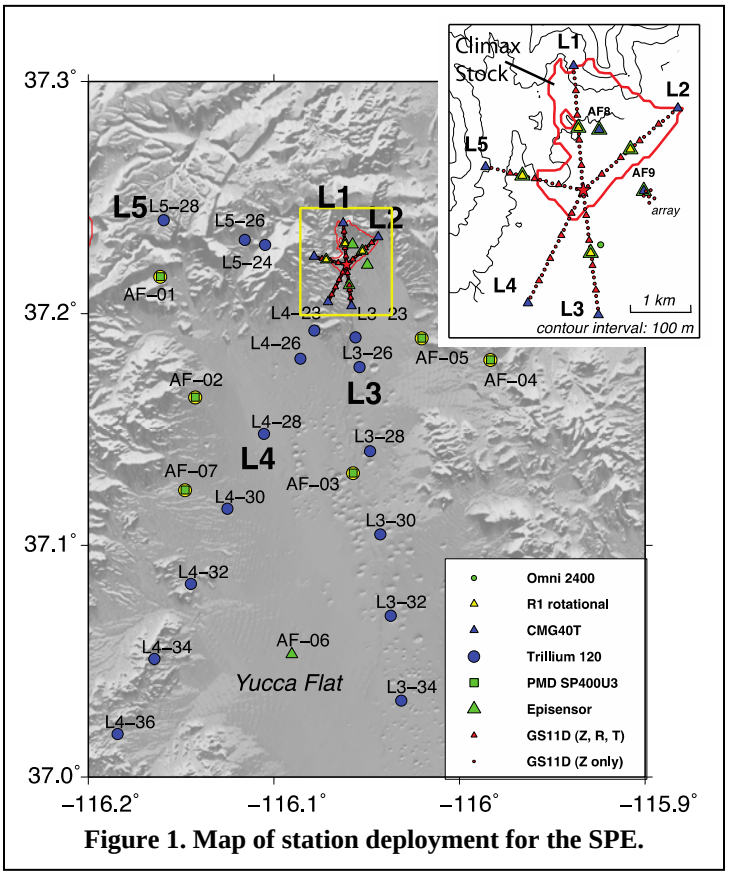

Figure 1. Map of station deployment for the SPE.

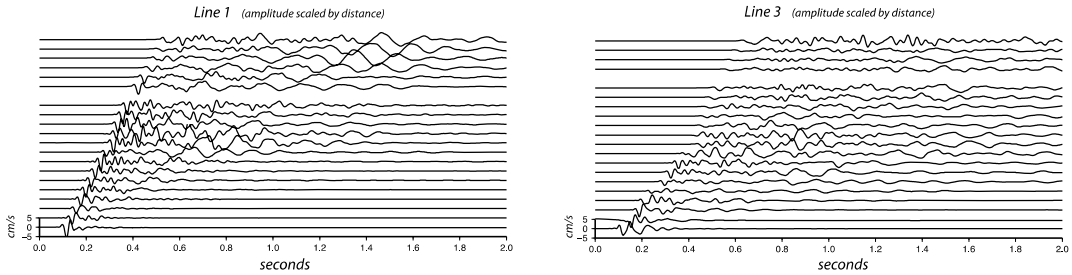

Figure 2. Recorded vertical velocity at L1 (left) and L3 (right).

Climax Stock to the sediments and tuffs of Yucca Flat.

To assist understanding of the waveforms, a polarization filter (Vidale, 1986) is applied to selected waveforms at a distance of 400m (Figure 3). Plots of Strike and Dip are the estimated azimuth and dip angle of the direction of maximum polarization. Angular Polarization P_E measures the degree of ellipticity of motion. P_E is1 for circularly polarized motion, and P_E is 0 for linearly polarized motion. Polarization Strength measures the directionality of the particle motion. Polarization strength is high for motion highly polarized in a single direction.

L1-04 and L2-04 waveforms are similar and show a large amplitude, linearly polarized phase observed in the transverse component, with its peak at 0.15s, travelling with a very small strike angle, which we interpret as a direct S body wave from the source. The second and third arrivals observed on all three components (peak amplitudes at 0.30 s and 0.38 s at L1-04 and L2-04) appears to be an elliptically polarized Rayleigh wave propagating from the source direction as indicated by angular polarization, and low strike angle and dip angles. The fourth significant phase observed in the transversal component which starts at 0.42 s and 0.5 sec at L1-04 and L2-04, respectively is a Love wave. Later phases are scattered surface waves. For L3-04, which is in Yucca Flat, the pattern differs. The first energetic arrival is a strong SV wave immediately followed by a Rayleigh wave. The largest phases at this station are multi-azimuthal Love waves.

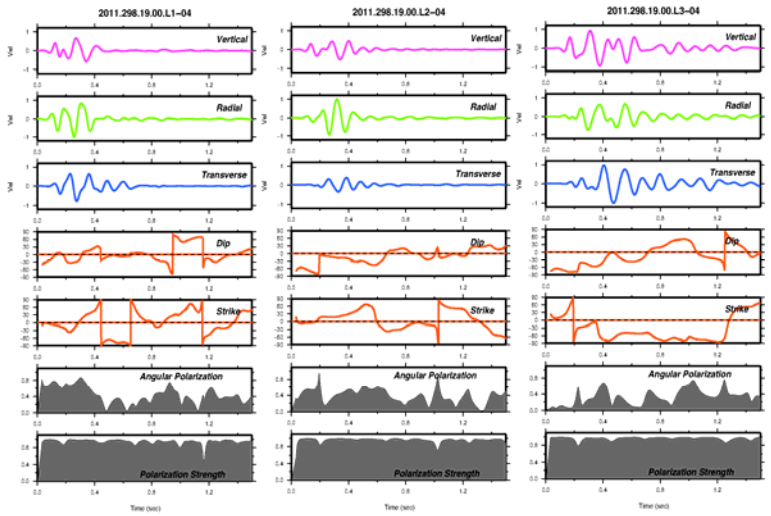

Figure 3. Polarization analysis of the velocity records at stations L1-04, L2-04, and L3-04. The Dip Strike Angular Polarization and Polarization Strength are defined in the text.

Waveform Moment Tensor Inversion

As a preliminary step towards evaluating the source mechanism of the SPE-2 explosion we conducted a full moment-tensor inversion using waveform data recorded by broadband instruments (Guralp CMG-40T and Trillium-120). We applied the inversion technique of Ford et al (2006). Synthetic displacement seismograms are calculated with a frequency-wavenumber integration method. Both computed and recorded displacements were band-pass filtered at 0.5-2Hz. A 1D velocity model was constructed assuming a 20 m thick weathered layer (Vp = 2700 m/s, Vs = 1600, r = 2600 kg/m^3, Q = 300) over granite (Vp = 5000 m/s, Vs = 2700 m/s, r = 2600 kg/m3, Q = 600).

Inversions were conducted using four possible source types: explosion, full moment tensor, deviatoric, and double-couple (Table 1). The explosion source fit the vertical components reasonably well except for station L3-20, which is located on the alluvium and tuffs of Yucca Flat rather than the granite Climax Stock. Radial components appeared similar in shape but with a poor fit to the amplitudes. As expected for a 1D model and isotropic source, no energy was generated on the tangential components. A full moment tensor inversion (Figure 4) provided a slightly better fit with a variance reduction of 49%. The moment tensor is partitioned into 75%, 20% and 5 % isotropic, CLVD and deviatoric components respectively. A constraint solution to only produce the deviatoric component yielded 68% CLVD and 32% DC contributions. None of these solutions fits the tangential displacement satisfactorily. This, combined with the observations of multi-pathing, suggest that a 3D model is required to adequately fit the data even in the low frequency range of 0.5 – 2 Hz.

Table 1. Results from 1D inversion

Source	*Variance reduction*	*Moment*	*Mw*
SPE2			
Explosion	45%	$M_0 6.3\times10^{11}$ N-m	$M_W 1.8$
Full moment tensor	48%	$M_0 2.1\times10^{12}$ N-m	$M_W 2.2$
Deviatoric	42%	$M_0 4.1\times10^{11}$ N-m	$M_W 1.7$
Best double couple	36%	$M_0 3.1\times10^{11}$ N-m	$M_W 1.6$
SPE1			
Explosion		$M_0 6\times10^{10}$ N-m	$M_W 1.2$

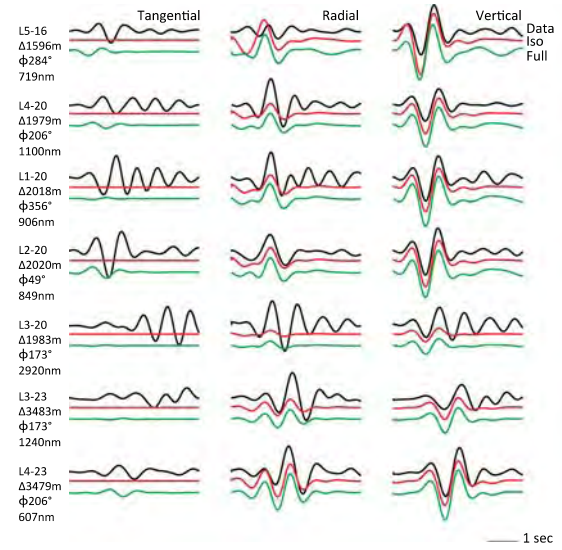

Figure 4. Waveform fits comparing data (black) with inversion results for the full moment tensor (green) and isotropic explosion (red) solution as matched at selected broadband stations.

___ 1 sec line plotted as a 1-sec scale to indicate duration of seismograms.

Iso and Full represent synthetics obtained with the isotropic and full moment tensor source representations.

Local 3D Velocity Model

An important part of our work is the development of a regional three-dimensional velocity model of the SPE site area. The model was used to simulate near-field ground motion from the SPE-2 explosion and perform sensitivity analysis of the simulated motion to shallow structure complexities and surface topography. Our velocity model was based on a geologic model developed with EarthVision, a 3D geologic GIS/visualization program (Figure 5). A set of layers corresponding to the topography, Quaternary alluvium, Tertiary tuffs, pre-Tertiary carbonates, and granite Climax Stock were meshed with an initial grid spacing of 10 m. Each layer was assigned a velocity with a vertical gradient and lateral and vertical variations. We used borehole data from the Climax stock and other locations in the Yucca flat to constrain the velocity gradient and vertical variability of velocity in the alluvium tertiary layer and granite. The horizontal and vertical correlation length of large-scale velocity variations within each layer are 350 m and 20 m respectively, whereas the amount of variability changes within each layer. We used the empirical relationships of Brocher (2005) to estimate the shear wave velocity and density from compressional wave velocity. Figure 6 shows a N-S cross-section of the 3D velocity model. The section passes through the SPE site. 1D profiles of the Vp shown at two locations illustrate the assumed gradient and vertical variation of velocity in the Climax Stock and Yucca flat.

A comprehensive geological study of the Climax stock that includes ample information from borehole data (Townsend et al., 2012) suggests that the granite is highly fractured and its top 30 m highly altered. Recent 2D tomographic models indicate that the thickness of the weathered layer is about 25 m with P wave

velocity of about 1.2 km/s at the surface. Patton et al. (2012) (this proceedings) found that the weathered layer along L1 has a thickness of 22 m, Vp=1300m/s and Vs=700 m/s. To investigate the effects of the weathered granite layer on seismic waveforms, we generated as series of 2.5D finite difference seismograms using an isotropic point source. The assumed velocity profiles and the corresponding simulation results for L1 are shown in Figure 7. Model #4 produces a good fit between the simulated and recorded Rg wave but underpredicts the Rg wave velocities slightly.

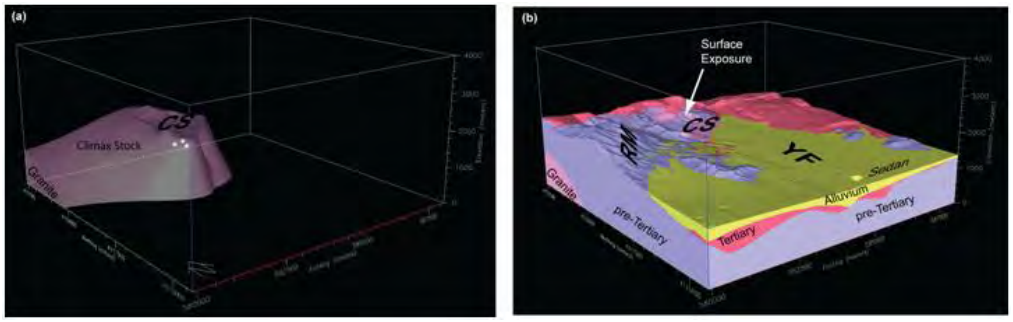

Figure 5. Geologic model used to develop the velocity model showing (a) granite Climax Stock and (b) pre-Tertiary, alluvium and fill in Yucca Flat (Rodgers et al., 2010a).

Finite Difference Simulation of Far-Field Ground Motion

A series of 3D simulations of the far-field wavefield were performed using the WPP finite difference code (Petersson and Sjogreen 2011). WPP is a second-order node-centered code designed specifically for implementation on highly-parallel machines. It models the full wave equation and is capable of handling 3D variations in the material properties, topographic variations on the free-surface (Appelo and Petersson, 2009), and attenuation (Petersson and Sjogreen, 2012). It also includes depth-dependent mesh refinement (Petersson and Sjogreen, 2010). WPP has been previously used to simulate earthquakes (Rodgers et al., 2008) and nuclear explosions (Rodgers et al., 2010b).

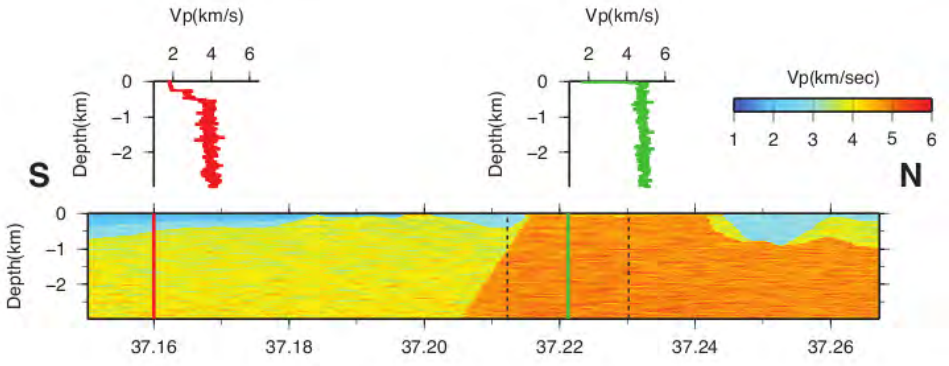

Figure 6. N-S cross-section of the 3D velocity model through the SPE site. Top panels show Vp as a function of depth at Yucca Flat (red line) and SPE site (green line).

The simulations of the SPE2 explosion were conducted on two computational domains, 8×8×5 km and 2×2×4. The grid spacing was variable in the vertical direction, and constant in both horizontal directions. The smallest grid spacing (5 m) corresponded to an upper frequency of about 10 Hz (minimum shear wave velocity was 700 m/s). In all simulations the explosion source was modeled as an isotropic point source with a Gaussian source time function and a seismic moment $Mo=2.0\times10^{12}$ Nm. Several simulations were run to investigate the effect of source time function, velocity variations, and surface topography. Simulations with a Mueller Murphy source time function (Mueller and Murphy, 1971) calculated for granite, source depth=45 m, yield=0.002 kT, Vp=5000m/s, Vs=2900 m/s and density=2.5 g/cm^3 produced the same results as simulations with a Gaussian source time function and a seismic moment $Mo=2.0\times10^{12}$ Nm in the considered frequency range of 0.1-10 Hz.

Figure 8 compares data and synthetics stations on granite along L1 and L2 in the frequency range of 0.1-10 Hz and between distances ranges of 200 m to 1000 m. The amplitude and phase of the Rg waves are very well reproduced for the vertical component. Rg on the radial component has a stronger reverberation in the synthetics than the data. Notice that the shear waves observed in the transverse component are not reproduced by the simulation well, as they arrive much later than the observed shear wave. Our simulation with an isotropic explosion source suggests that wave scattering in the source area did not contribute to the generation of shear waves observed in the transverse component, which may indicate a source contribution.

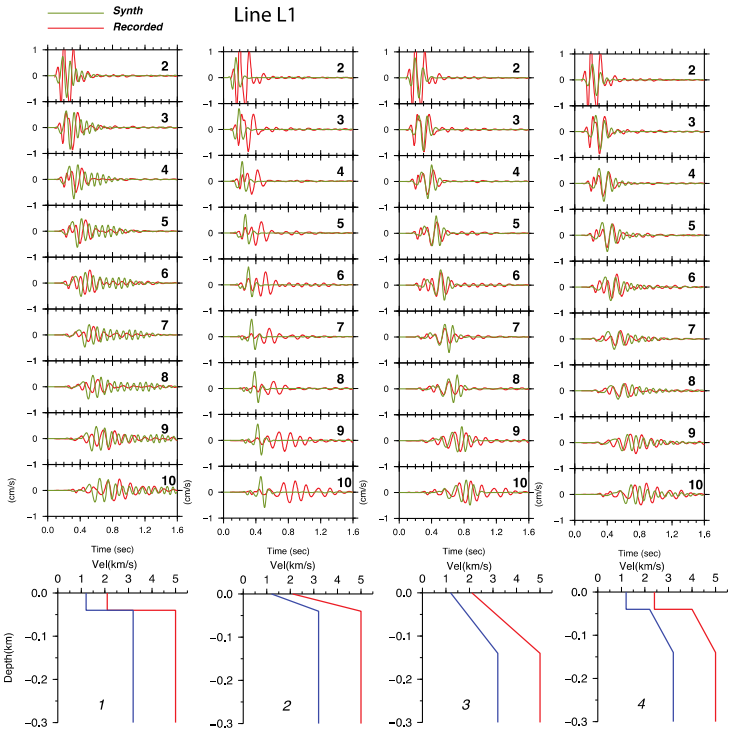

Figure 7. Simulated effects of surface weathering of the Climax stock granite on far-field waveforms (0.1-10 Hz). Each panel compares 2.5D finite difference synthetic seismograms (green) with recorded velocity waveforms (red) at stations along line L1. Bottom panels show the two-dimensional velocity models.

The inclusion of the weathered layer and surface topography has a dramatic effect on the synthetic seismograms. Figure 9 compares synthetics produced with 3D velocity models with and without topography. The topography has an effect on Rg waves observed in the radial and transverse components. The effect of topography is increased by a low velocity weathered layer. Figure 10 shows a snapshot of the wavefield simulated with a 3D velocity model that covers an area of 8 km × 8 km. The simulation shows that the complex geology and topography of the area is expected to cause strong variations in azimuth in both travel-time and waveform. In particular, as the seismic waves propagate to the south and southeast they encounter the low velocities of the Yucca Flat alluvium and underlying tuff. We are working to improve our model in these areas.

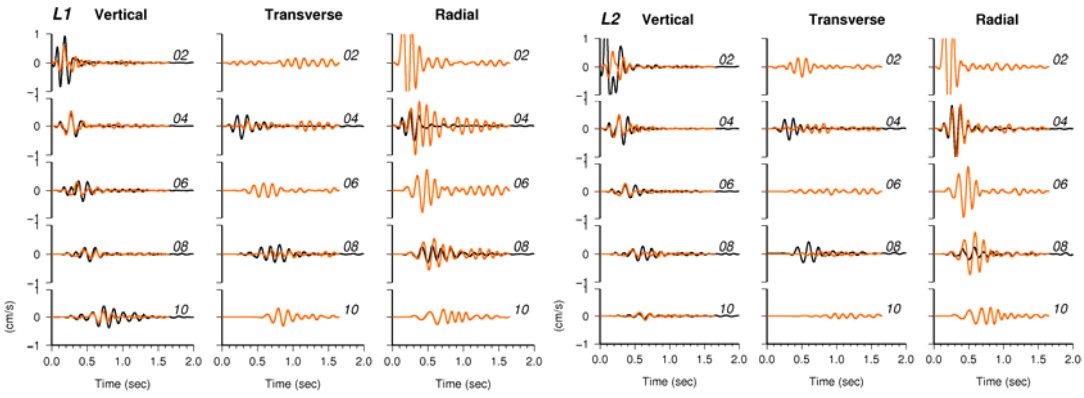

Figure 8. Comparison of data (black) and synthetics (brown) calculated using an isotropic point source model of the SPE-2 shot at stations array L1 (left) and L2 (right) (filtered, 0.1-10 Hz). The synthetics are calculated using a 3D velocity model with surface topography.

Coupling of 3D Hydrodynamic Source Modeling With far-field Anelastic Wave Propagation Modeling

Understanding the partitioning of energy excited by underground explosions as observed in the far-field, requires the ability to model both the near-field, which includes the nonlinear deformation and damage caused by the explosion, and the far-field, which consists of three-dimensional wave propagation in a

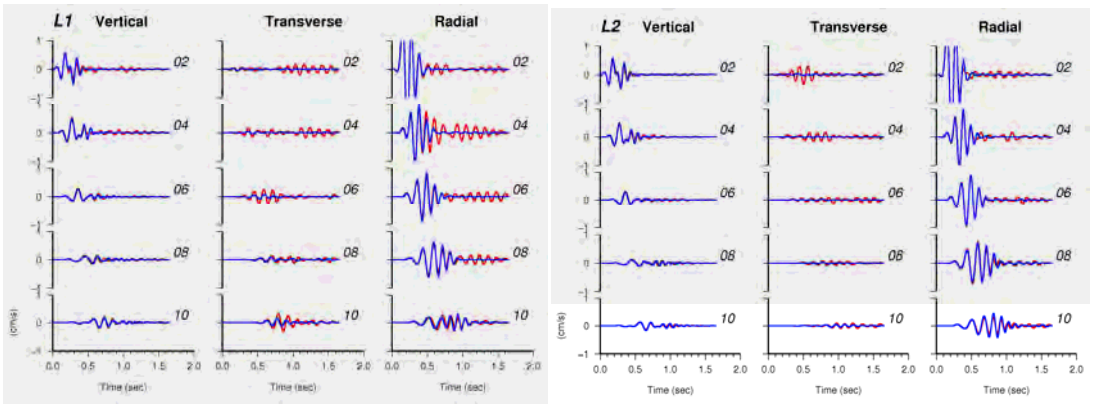

Figure 9. Effects of surface topography. Comparison of synthetic velocity seismograms calculated with surface topography (red traces) and without surface topography (blue traces) band-pass filtered at 0.1-10 Hz.

complex geological structure. We are developing an end-to-end three-dimensional (3D) simulation methodology to handle both near- and far-complex geological structure. The transition between hydrodynamic to seismic motion near the source is performed by coupling GEODYN, an Eulerian hydrodynamics code with adaptive mesh refinement, and WPP a finite-difference computer program.

Figure 11 illustrates an example of synthetic seismograms from an isotropic explosion source calculated with WPP and the coupled 3D-GEODYN-WPP codes using 3D simulations for a half space. The coupling between the two codes is performed on the faces of a cube of 100m × 100 × 100m centered at the source. Our next step is to perform simulations using realistic models of the nonlinear deformation and damage caused by the chemical explosion (Antoun et al., these Proceedings).

Physical Models for P/S Earthquake-explosion Discrimination

The far-field seismic sensors in and around NNSS record natural earthquakes in addition to the SPE chemical explosions. Previously (Mellors et al., 2011), we showed a comparison of the SPE-1 shot to a nearby magnitude 0.7 earthquake at a few of the SPE seismic stations filtered at a high frequency passband of 16-32 Hz. These seismograms show the expected difference in relative P/S amplitude values for closely located and similar sized events, with the explosion having systematically higher P/S amplitudes than the earthquake. This P/S discriminant has shown empirically that it can separate explosions from a background of earthquakes at many locations in the world (e.g., Dysart and Pulli, 1987; Baumgardt and Young, 1990; Walter et al., 1995; Taylor, 1996; Hartse et al., 1997; Battone et al.; 2002; Walter et al., 2007).

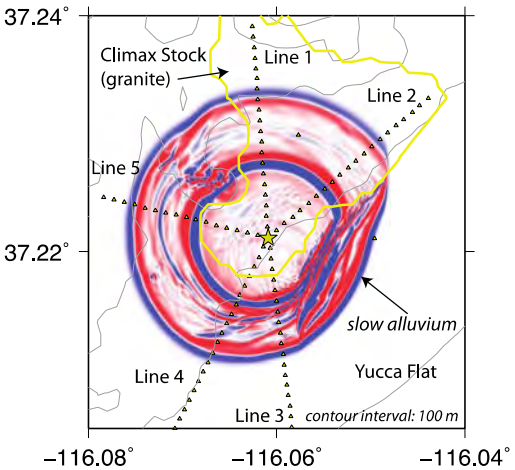

Figure 10. Snapshot of the SPE simulated wavefield using WPP program and a 3D velocity model with surface topography.

For the SPE we are trying to address questions of how and why the P/S discriminant works. This includes investigating any magnitude, frequency, depth or other dependencies that could affect how to use the discriminant in practice. We are also working towards understanding the separate contributions of source and path on the discriminant through the development of physics-based models. A question we are trying to address in the SPE is how much of such observed differences are due to source parameter differences (e.g., mechanism, duration), versus how much is due to path differences (e.g., depth, scattering). In order to apply the P/S discriminant over broad regions we need to be able to model and account for such effects.

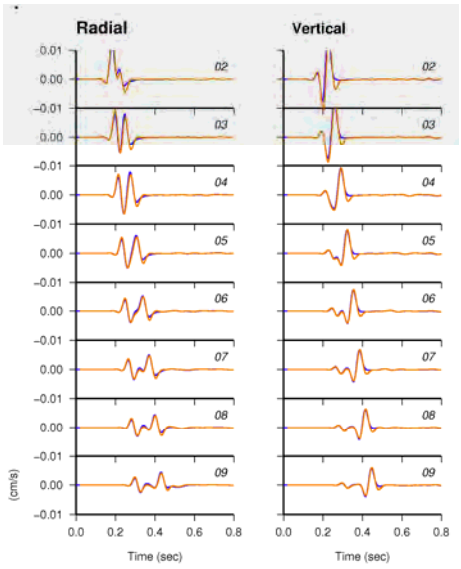

Figure 11. Comparison of synthetic velocity seismograms calculated with WPP code (brown) GEODYN-WPP codes (blue), for a half space velocity model. The seismograms are band-pass filtered at 0.1-13 Hz

We are using the SPE data to test earthquake and explosion models. For example in Figure 12 we show the SPE-1 and SPE-2 data at one of the SPE stations. Note that at low frequency, below the corner frequency of the two events, the seismograms are very well correlated and the amplitude difference is very close to the factor of ten change in the yield. We form spectral ratios based on energy in the P-wave arrival window on the vertical component and the S-wave arrival window on the transverse component. We compare these observed ratios with several explosion source models. For example in Figure 12 we calculate the expected P-wave source spectral ratio for SPE-2 to SPE-1 using the Muller and Murphy (1971) model for granite with the parameters given by Steven and Day (1985). We used the actual depths of the shots and an assumed factor of two enhancement in yield for the chemical explosion (compared to the nuclear explosion for which the model was developed). The match of the model with the observations at one station is reasonable.

We also calculated the expected SPE-2 to SPE-1 ratio for S-waves using the Fisk (2006) conjecture that the S-waves are matched by lowering the Mueller-Murphy corner frequency by the ratio of the P to S wave velocity. The implication of this model is that S-waves are generated close to the source and are tied to the elastic radius similarly to P-waves. As shown in Figure 12, the fit to the ratio of the observed S-wave ratios at this station is poor. It is not clear yet if the observed ratio reflects the true S-wave source or is contaminated at high frequencies by scattered P and other waves. We are actively working to better model and separate path and source effects in order to gain insight into the true source model for explosion S-waves. Such a model is crucial to being able to understand both the basis for the P/S ratio discriminants and the circumstances under which they may not work.

CONCLUSIONS AND RECOMMENDATIONS

Results from our initial analysis of recorded and simulated waveforms from the SPE-2 explosion demonstrate that the waves generated from the explosion have a rich content in shear wave energy. The S-P wave conversion at the surface topography, and affected by the weathered layer in the Climax stock contributed to generation of Rg waves near the source region. However the shear waves observed in the transverse component arrive much earlier than near-source scattered waves. Our interpretation of these results is that the origin of such waves is at the source. We have developed the computational capability that will allow modeling of nonlinear deformation and damage caused by the explosion, as well as three-dimensional wave propagation effect in a complex geological structure. We will use these tools to model near- and far-field data to better distinguish source and path effects. A full suite of other analysis will be conducted. This will include further study of the rotational data and modeling, small array signal processing, examination of the P, S wave spectra and ratios, body and surface wave amplitudes, full moment tensor inversion using 3D Green's functions, interferometry, and comparison with local earthquake data.

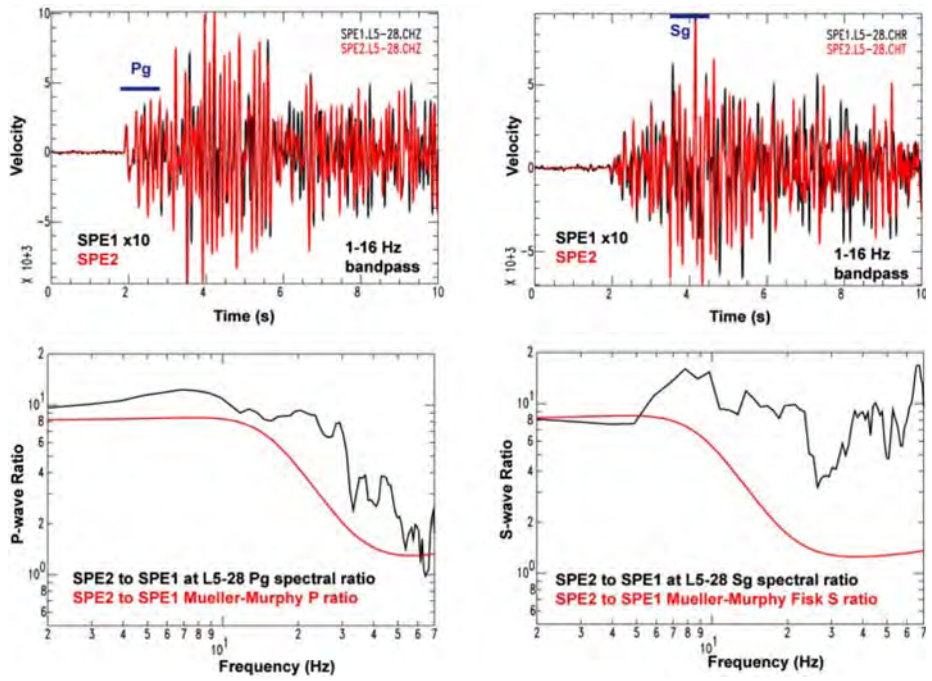

Figure 12. A comparison of the SPE-1 and SPE-2 chemical explosion seismograms at station L5-28 about 9 km away. Upper right shows the vertical component, and the upper left shows the transverse component (SPE-1 L5-28 had an error in the horizontal orientation). Sseismograms are band pass filtered from 1-16 Hz and the 100kg SPE1 data is multiplied by a factor of 10 and correlates very well with the 1000 kg SPE-2 shot. The lower left shows the Pg window spectral ratio for SPE-2/SPE-1 which matches well with the Muller-Murphy prediction but the Sg window spectral ratio (lower right) does not match the Fisk (2006) conjecture prediction well possibly due to scattering and contamination.

ACKNOWLEDGEMENTS

We thank NA-22 and all the SPE participants for all their efforts in planning and carrying out SPE-1 and SPE-2. We thank the group at NSTec and, in particular, Bob White and Catherine Snelson-Gerlicher for their efforts. Rob Abbott and Margaret Townsend were also very helpful. Gabe Plank and Ken Smith assisted with data organization. Numerical simulations were performed on the SIERRA and CAB Linux clusters operated by Livermore Computing using a Computing Grand Challenge Allocation.

REFERENCES

Antoun, T., X. Heming, O. Y. Vorobiev, E. B. Herbold, L. Glenn, and I. Lomov (2012). Analysis and simulation of near-field wave motion data from the source physics explosions, these Proceedings.

Appelo D. and N. A. Petersson (2009). A stable finite difference method for the elastic wave equation on complex geometries with free surfaces, *Comm. Comput. Phys.* **5**, 84–107.

Battone, S., M. D. Fisk and G. D. McCarter (2002). Regional seismic-event characterization using a Bayesian formulation of simple kriging, *Bull. Seismol. Soc. Am.* **92**, 2277–2296.

Baumgardt, D. R. and G. B. Young (1990). Regional seismic waveform discriminants and case-based identification using regional arrays, *Bull. Seismol. Soc. Am.* **80**, 1874–1892.

Brocher, T. M. (2005). Empirical relations between elastic wavespeeds and density in the earth's crust. *Bull. Seismol. Soc. Am.* **95**, 2081–2092.

Brunish, W. N., W. L. Hawkins, D. Coblentz, H. J. Patton, J. J. Zucca, J. J. Sweeney, C. R. Carrigan, T. H. Antoun, C. E. Seifert, K. H. Wohletz, C. R. Bradley, A. J. Sussman, T. W. Bowyer, R. Cirbell, C. M. Snelson, and P. Lee (2010). Source physics experiments at the Nevada Test Site, in *Proceedings of the 2010 Monitoring Research Review: Ground-Based Nuclear Explosion Monitoring Technologies*, LA-UR-10-05578, Vol. 1, pp. 370–390.

Dysart, P. S. and J. J. Pulli (1987). Spectral study of regional earthquakes and chemical explosions recorded at the NORES array. SAIC technical report C87-03.

Fisk, M.D (2006). Source spectral modeling of regional P/S discriminants at nuclear test sites in China and the Former Soviet Union, *Bull. Seismol. Soc. Am.* **96**, 2348–2367.

Ford, S. R., D. S. Dreger, and W. R. Walter (2006). Identifying isotropic events using an improved moment tensor technique, in *Proceedings of the 28th Seismic Research Review: Ground-Based Nuclear Explosion Monitoring Technologies*, LA-UR-06-5471, Vol. 1, pp. 590–596.

Hartse, H., S. R. Taylor, W. S. Phillips, and G. E. Randall (1997). A preliminary study of regional seismic discrimination in Central Asia with an emphasis on Western China, *Bull. Seismol. Soc. Am.* **87**, 551–568.

Mellors, R., A. J. Rodgers, P. E. Harben, W. R. Walter, S. Ford, J. L. Wagoner, N. A. Petersson, B. A. Sjogreen, T. F. Hauk, S. D. Ruppert, Stephen C. Myers, E. M. Matzel, Douglas A. Dodge, M. E. Pasyanos, and J. P. Lewis (2011). Analysis and simulation of far-field seismic data from the Source Physics Experiment explosions, in *Proceedings of the 2011 Monitoring Research Review: Ground-Based Nuclear Explosion Monitoring Technologies*, LA-UR-11-04823, Vol. 1, pp. 503–512.

Mueller, R. A. and J. R. Murphy (1971). Seismic characteristics of underground nuclear detonations. Part I. seismic spectral scaling, *Bull. Seismol. Soc. Am*. **61,** 1675–1692.

Petersson, N.A. and B. Sjogreen (2010). Stable grid refinement and singular source discretization for seismic wave simulations, *Comm. Comput. Phys.* **8**(5), 1074–1110.

Petersson, N.A., B. Sjogreen (2011). User's guide to WPP version 2.1, Lawrence Livermore National Laboratory, LLNL-SM-487431

Petersson, N.A. and B. Sjogreen (2012). Stable and efficient modeling of anelastic attenuation in seismic wave propagation, *Comm. Comput. Phys.* **12**(1), pp. 193-225, DOI: 10.4208.

Rodgers, A., A. Petersson, S. Nilsson, B. Sjogreen and K. McCandless (2008). Broadband waveform Modeling of Moderate Earthquakes in the San Francisco Bay Area to Evaluate the USGS 3D Seismic Velocity Model, *Bull. Seismol. Soc. Am*. **98**, 969–988.

Rodgers, A. J., J. Wagoner, N. A. Petersson, and B. Sjogreen (2010a). Pre-shot simulations of far-field ground motions for the Source Physics Experiment (SPE) explosions at the Climax Stock, Nevada National Security Site, Lawrence Livermore National Laboratory technical report LLNL-TR-461990.

Rodgers, A., N. A. Petersson, B. Sjogreen (2010b). Simulation of topographic effects on seismic waves from shallow explosions near the North Korean Nuclear Test Site with emphasis on shear wave generation, in press *J. Geophys. Res.-B Solid Earth Planets*, doi:10.1029/2010JB007707, LLNL-JRNL-433892.

Taylor, S. (1996). Analysis of high-frequency Pg/Lg ratios from NTS explosions and Western U.S. earthquakes, *Bull. Seismol. Soc. Am.* **86**, 1042–1053.

Townsend, M., L.B. Protho, and C.Obi (2012). Geology of the Source Physics Experiment site Climax stock, Nevada National Security Site. DOE/NV/25946-1448.

Vidale, J.E (1986). Complex polarization analysis of particle motion. *Bull. Seismol. Soc. Am*. **76**, 1393–1405.

Walter, W. R., K. Mayeda, and H. J. Patton, (1995). Phase and spectral ratio discrimination between NTS earthquakes and explosions Part 1: Empirical observations, *Bull. Seismol. Soc. Am.* **85**, 1050–1067.

Walter, W. R., E. Matzel, M. Pasyanos, D. Harris, R. Gok and S. Ford (2007). Empirical observations of earthquake explosion discrimination using P/S ratios and implications for the source of explosion S-waves, in *Proceedings of the 29th Seismic Research Review*: *Ground-Based Nuclear Explosion Monitoring Technologies*, LA-UR-07-5613, Vol. 1, pp. 684–693.